Eur. Phys. J. B **29**, 441–455 (2002)
DOI: 10.1140/epjb/e2002-00325-4

THE EUROPEAN PHYSICAL JOURNAL B

Towards finite-dimensional gelation

K. Broderix[†], M. Weigt[a], and A. Zippelius

Institut für Theoretische Physik, Universität Göttingen, Bunsenstr. 9, 37073 Göttingen, Germany

Received on 24 April 2002
Published online 14 October 2002 –

Abstract. We consider the gelation of particles which are permanently connected by random crosslinks, drawn from an ensemble of finite-dimensional continuum percolation. To average over the randomness, we apply the replica trick, and interpret the replicated and crosslink-averaged model as an effective molecular fluid. A Mayer-cluster expansion for moments of the local static density fluctuations is set up. The simplest non-trivial contribution to this series leads back to mean-field theory. The central quantity of mean-field theory is the distribution of localization lengths, which we compute for all connectivities. The highly crosslinked gel is characterized by a one-to-one correspondence of connectivity and localization length. Taking into account higher contributions in the Mayer-cluster expansion, systematic corrections to mean-field can be included. The sol-gel transition shifts to a higher number of crosslinks per particle, as more compact structures are favored. The critical behavior of the model remains unchanged as long as finite truncations of the cluster expansion are considered. To complete the picture, we also discuss various geometrical properties of the crosslink network, *e.g.* connectivity correlations, and relate the studied crosslink ensemble to a wider class of ensembles, including the Deam-Edwards distribution.

PACS. 61.43.-j Disordered solids – 64.70.Dv Solid-liquid transitions – 61.41.+e Polymers, elastomers, and plastics 05.20.Jj Statistical mechanics of classical fluids

1 Introduction

In this paper we study chemical gelation, *i.e.* the equilibrium transition from a liquid (sol) to an amorphous solid (gel) which is induced by the introduction of permanent random crosslinks between the particles of the liquid. The classical theory of gelation, as developed by Flory and Stockmayer [1], assumes a tree like connectivity of the random macromolecular networks generated in the process of gelation and vulcanization. The critical exponents are those of mean-field percolation. Stauffer [2] and de Gennes [3] used instead the lattice connectivities of finite dimensional percolation, embedding the gelation transition in the context of critical phenomena. The resulting critical exponents are those of three-dimensional percolation theory, in contradiction with the classical values. Experimental support has accumulated for the non-classical values [4] and, in addition, given evidence for the size of the critical region, outside of which mean-field exponents prevail [5]. One concludes that the geometric connectivity of gels is well described by percolation theory. On the other hand, the thermal properties of gels are beyond the scope of percolation theory and have in recent years been addressed with statistical mechanics, considering both geometric and thermal fluctuations [6–10]. A mean-field picture has been developed [11–13] and a renormalization group analysis [14,15] has been carried out for the fluid side of the transition. Thereby the approach of statistical mechanics has been connected to percolation theory. However, the structural and elastic properties of finite-dimensional gels are still only known within mean-field theory.

In this paper we focus on the *gel* phase for an ensemble of crosslinks, which is given by continuum percolation. This is *not* the Deam-Edwards distribution [6], which has been used frequently in the statistical approach. After a short introduction of the model in Section 2, we discuss geometrical properties of the network, generated by three-dimensional percolation, *e.g.* we investigate correlations in connectivity of neighboring sites and compute the number of small loops (Sect. 3). Subsequently we set up a Mayer-cluster expansion for the crosslinked melt (Sect. 4). Our effort is not directed towards the critical behavior of the gelation transition, which was studied in references [14,15]; rather we want to find out, whether the characteristics of the gel phase as described by mean-field theory, survive in a finite-dimensional model. We recall that already on the level of a mean-field theory one needs a distribution of length scales to characterize the local static density fluctuations of the gel phase. Our aim

[a] e-mail: weigt@theorie.physik.uni-goettingen.de
[†] deceased

is to find out in how far this picture has to be modified in a short-range model.

The lowest diagram of the Mayer cluster expansion leads back to mean-field theory (Sect. 5), which is expected to be appropriate deep in the gel phase away from the transition point. We compute the distribution of localization lengths for all connectivities. For the strongly connected gel we find a multi-peak structure of the distribution, such that each coordination number corresponds, to leading order, to a well-defined localization length. Subsequently the first correction to mean-field theory within the Mayer-cluster expansion is calculated. The critical connectivity is increased due to the existence of small loops, which do not increase the cluster size. The gel fraction and the distribution of localization lengths change only quantitatively, as compared to mean-field theory and the critical exponents remain the same as long as we only consider bare perturbation theory and do not resum the Mayer-cluster expansion. Finally in Section 6, we discuss a general class of crosslink distributions, which includes the Deam-Edwards distribution as well as the distribution of d-dimensional percolation.

2 The model: crosslinked point particles

We consider a system of N identical classical particles, confined to a d-dimensional volume V with the average density of particles $\rho_0 = N/V$ being constant in the thermodynamic limit $N, V \to \infty$. The particle positions are denoted by $R = \{\mathbf{R}_i\}$, with i running from 1 to N. The interactions are given by the Hamiltonian

$$H(R) = U(R) + \sum_{e=1}^{M} V(\mathbf{R}_{i_e} - \mathbf{R}_{j_e}) \; . \tag{1}$$

Here, $U(R)$ describes the particle interactions in the fluid, without crosslinks, and is given by a sum over single-particle and pair potentials. Permanent random crosslinks are introduced between M pairs of particles, numbered by $\{(i_e, j_e)\}_{e=1}^{M}$. Two monomers, participating in a crosslink, are forced to remain close to each other. We model this constraint by an attractive pair potential $V(\mathbf{R}_{i_e} - \mathbf{R}_{j_e})$. The simplest choice is a harmonic one, $V(\mathbf{R}_{i_e} - \mathbf{R}_{j_e}) = \frac{\kappa}{2}(\mathbf{R}_{i_e} - \mathbf{R}_{j_e})^2$, where κ is the strength of the crosslink coupling. It has been shown that the harmonic potential is equivalent to crosslinks represented by hard constraints in the limit $\kappa \to \infty$ [16]. Note that further geometrical constraints arise indirectly *via* the interlocking of closed loops of crosslinks, see the discussion in [13]. These effects are not taken into account in the above Hamiltonian.

It is convenient to introduce the symmetric $N \times N$ connectivity matrix J with entries

$$J_{ij} = \sum_{e=1}^{M} (\delta_{i,i_e}\delta_{j,j_e} + \delta_{i,j_e}\delta_{j,i_e}) \; . \tag{2}$$

These entries equal one, whenever i and j are linked together, and zero otherwise. Multiple crosslinks are excluded. Harmonic interactions due to the crosslinks can thus be represented by

$$\sum_{e=1}^{M} V(\mathbf{R}_{i_e} - \mathbf{R}_{j_e}) = \frac{\kappa}{2} \sum_{1 \le i < j \le N} J_{ij}(\mathbf{R}_i - \mathbf{R}_j)^2 \; . \tag{3}$$

The thermal degrees of freedom are the positions of the monomers. The set of crosslinks $\mathcal{C} := \{(i_e, j_e)_{e=1}\}$ represents the quenched disorder of the model, so that the monomers equilibrate in the presence of a fixed, non-equilibrium configuration of crosslinks.

All thermodynamic properties can be obtained from the partition function

$$Z(\mathcal{C}) = \int_{V^N} \mathrm{d}^{dN} R \; \exp\{-\beta H\} \tag{4}$$

which still depends on the quenched disorder $\mathcal{C}$. Here $\beta = 1/(k_B T)$ denotes the inverse temperature. One usually assumes that the Gibbs free energy, $\beta F = -\log Z$, is self-averaging in the thermodynamic limit, and thus computes its average over all crosslink realizations, $\overline{F}$.

3 Distribution of Crosslinks: Finite-dimensional percolation

In this section, we give an explicit formula for the distribution of crosslinks corresponding to d-dimensional percolation. It is based on the intuitive picture that a given number of crosslinks M is introduced simultaneously and instantaneously into the fluid of monomers. The crosslinks are strictly bivalent and connect pairs of monomers by a chemical bond. Given the instantaneous (or more realistically fast) reaction, pairs of monomers which are nearby in the instant of crosslinking, have a high probability to be connected, whereas pairs of monomers which are distant, have a very small probability to be crosslinked. The assumption of a fast crosslinking reaction as compared to the diffusive time-scale of the fluid molecules is realistic and becomes better and better the closer one gets to the gelation transition, because larger and larger clusters are built up and give rise to increasingly longer relaxation times of the molecules in the fluid.

The distribution is generated in two steps:

(1) A liquid configuration $R^0 = \{\mathbf{R}_i^0\}_{i=1}^N$ (an instant) of a d-dimensional fluid is generated, by randomly choosing N points in d-dimensional space. One possibility is to generate liquid configurations with the Boltzmann weight of the uncrosslinked system, thereby including short-range correlations of the fluid. Such a procedure will be discussed in Section 6. Here we consider the simpler case of random, uncorrelated positions $R^0 = \{\mathbf{R}_i^0\}_{i=1}^N$ in order to model crosslinks corresponding to d-dimensional percolation.

(2) Given the configuration R^0, each crosslink is chosen independently, as described by a factorized distribution

$$P(\mathcal{C}|R^0) = \prod_{e=1}^{M} p(i_e, j_e|R^0). \tag{5}$$

The probability for a particular crosslink (i_e, j_e) depends only on the relative distance $|\mathbf{R}^0_{i_e j_e}|$

$$p(i_e, j_e|R^0) = \frac{\Delta(|\mathbf{R}^0_{i_e j_e}|)}{\sum_{i,\,j=1}^{N} \Delta(|\mathbf{R}^0_{ij}|)} \tag{6}$$

with $\mathbf{R}^0_{ij} = \mathbf{R}^0_i - \mathbf{R}^0_j$. The function $\Delta(x)$ should be of finite range, examples are $\Delta(x) = \theta(\lambda - x)$ or $\Delta(x) = \mathrm{e}^{-x/\lambda}$. The denominator in equation (6) ensures the proper normalization. The average of an observable $f(R^0, \mathcal{C})$ over all crosslink configurations $\mathcal{C}$ is given by

$$\overline{f(R^0,\mathcal{C})} = \int_{V^N} \frac{\mathrm{d}^{dN} R^0}{V^N} \times \sum_{i_1,\,j_1=1}^{N} \cdots \sum_{i_M,\,j_M=1}^{N} P(\mathcal{C}|R^0)\; f(R^0,\mathcal{C})\;. \tag{7}$$

Note that the integration over R^0 is part of the averaging over all crosslink distributions and should not be confused with thermal averages.

Sometimes, it is technically simpler to allow the total number of crosslinks to fluctuate. To this end, we replace the second step in the above procedure by the following:

2′) Given the configuration R^0, choose each crosslink independently, as described by a factorized distribution

$$P(\{J_{ij}\}_{i<j}|R^0) = \prod_{1\le i<j\le N} \Big(\delta(J_{ij}-1)p(\mathbf{R}^0_{ij}) + \delta(J_{ij})(1-p(\mathbf{R}^0_{ij}))\Big) \tag{8}$$

which explicitely excludes multiple crosslinks. The function $p(\mathbf{x})$ should take values $0 \le p(\mathbf{x}) \le 1$ and be of finite range. It will be convenient to assume a Gaussian shape

$$p(\mathbf{R}^0_{ij}) = \exp\Big\{-\frac{a}{2}(\mathbf{R}^0_{ij})^2\Big\}\,. \tag{9}$$

The "crosslinking-length" $\ell = a^{-1/2}$ is chosen comparable to the mean distance between particles, $\rho_0^{-1/d}$, in order to guarantee an extensive number of crosslinks (see the following section). The average (7) of an observable over all crosslink configurations, now equivalently denoted by $\mathcal{C} := \{J_{ij}\}_{i<j}$, is then replaced by

$$\overline{f(R^0,\mathcal{C})} = \int_{V^N} \frac{\mathrm{d}^{dN} R^0}{V^N} \quad \int \prod_{i<j} \mathrm{d}J_{ij}\; P(\mathcal{C}|R^0)\; f(R^0,\mathcal{C})\;. \tag{10}$$

Before discussing the physics of the crosslinked system, we will investigate some geometrical properties of the network of crosslinks. Special emphasis is given to local structures which are characteristic for the low-dimensional structure of the network. They differ substantially from the properties of diluted random graphs [17] which give the proper mean-field description of the disorder distribution.

3.1 Number of crosslinks

To start with, we compute the distribution of the total number of crosslinks. As each pair of monomers is considered independently in the crosslinking process, the crosslink number is expected to fluctuate according to a Poissonian distribution. For the probability $W(M)$ of having M crosslinks we indeed find

$$\begin{aligned} W(M) &= \overline{\delta_{M,\sum_{i<j} J_{ij}}} \\ &= \int_{-\pi}^{\pi} \frac{\mathrm{d}x}{2\pi} \overline{\mathrm{e}^{\mathrm{i}x(M-\sum_{i<j} J_{ij})}} \\ &= \int_{-\pi}^{\pi} \frac{\mathrm{d}x}{2\pi} \mathrm{e}^{\mathrm{i}xM} \left(1 - \frac{W_-}{V} + \frac{W_-}{V}\mathrm{e}^{-\mathrm{i}x}\right)^{\binom{N}{2}} \\ &= \binom{\frac{N(N-1)}{2}}{M} \left(1-\frac{W_-}{V}\right)^{\frac{N(N-1)}{2}-M} \left(\frac{W_-}{V}\right)^M, \end{aligned} \tag{11}$$

where $W_- := \int_V \mathrm{d}^d R\; p(\mathbf{R}) = (2\pi/a)^{d/2}$ denotes the effective crosslinking volume for the distribution of equation (9). In the limit of large N, with constant particle density $\rho_0 = N/V$, these probabilities tend to a Poissonian

$$W(M) \to \frac{\overline{M}^M}{M!}\mathrm{e}^{-\overline{M}} \tag{12}$$

with mean $\overline{M} = \rho_0 W_- N/2$. Fluctuations around the mean are of order $\mathcal{O}(\sqrt{\overline{M^2} - \overline{M}^2}) = \mathcal{O}(\sqrt{\overline{M}})$, and hence small compared to $\overline{M}$. We therefore expect the differences between the ensembles with fixed and fluctuating number of crosslinks to disappear in the thermodynamic limit.

3.2 Distribution of coordination numbers

The simplest local property of the crosslink network is given by the distribution of coordination numbers. The average fraction of particles being connected to exactly k other particles is given by

$$\begin{aligned} w(k) &= \overline{\frac{1}{N}\sum_i \delta_{k,\sum_j J_{ij}}} \\ &= \overline{\delta_{k,\sum_j J_{ij}}} \\ &= \int_{-\pi}^{\pi} \frac{\mathrm{d}x}{2\pi} \overline{\mathrm{e}^{\mathrm{i}x(k-\sum_j J_{ij})}} \\ &= \int_{-\pi}^{\pi} \frac{\mathrm{d}x}{2\pi} \mathrm{e}^{\mathrm{i}kx} \left(1 - \frac{W_-}{V} + \frac{W_-}{V}\mathrm{e}^{-\mathrm{i}x}\right)^{N-1} \\ &= \binom{N}{k} \left(1-\frac{W_-}{V}\right)^{N-k} \left(\frac{W_-}{V}\right)^k \\ &\to \mathrm{e}^{-c}\frac{c^k}{k!}. \end{aligned} \tag{13}$$

where the last expression describes the limiting distribution for $N \to \infty$. It is thus found to equal a Poissonian of

mean $c := \rho_0 W_-$. The same coordinations are found in the long-ranged case $p(\mathbf{R}_{ij}^0) = c/N$. Differences to the long-ranged case show up in nonlocal features, as connectivity correlations and occurrence of loops.

3.3 Connectivity correlations

To study connectivity correlations, we consider the coordination numbers of particles which are directly connected by a single crosslink. Given a large network, we determine the (asymptotic) probability that a randomly and uniformly selected crosslink has endpoints of coordinations k_1 and k_2 respectively. This quantity is given by the sum over all links, which have one endpoint connected to k_1 and the other endpoint connected to k_2 particles, normalized by the total number of crosslinks

$$\begin{aligned} w(k_1,k_2) &= \frac{2}{\rho_0 W_- N} \sum_{i<j} J_{ij}\ \delta_{k_1,\sum_l J_{il}}\ \delta_{k_2,\sum_l J_{jl}} \\ &= \frac{2}{\rho_0 W_- N} \sum_{i<j} J_{ij}\ \delta_{k_1-1,\sum_{l\neq i,j} J_{il}}\ \delta_{k_2-1,\sum_{l\neq i,j} J_{jl}} \\ &= \frac{N-1}{\rho_0 W_-} \int_{-\pi}^{\pi} \frac{\mathrm{d}x_1\ \mathrm{d}x_2}{4\pi^2} \mathrm{e}^{\mathrm{i}x_1(k_1-1)+ix_2(k_2-1)} \\ &\quad \times \overline{J_{12}\mathrm{e}^{-\mathrm{i}\sum_{l\geq 3}(J_{1l}x_1+J_{2l}x_2)}}\ . \end{aligned} \tag{14}$$

The disorder distribution of equation (9) allows to compute the average up to summations

$$\begin{aligned} w(k_1,k_2) = & \sum_{n=0}^{\min(k_1,k_2)-1} \sum_{l=0}^{\infty} \sum_{m=0}^{k_1+k_2-2-2n} \binom{k_1+k_2-2-2n}{m} \\ & \times \frac{(-1)^m\ c^{k_1+k_2-2-n+l}\ \mathrm{e}^{-2c}}{n!\ (k_1-1-n)!\ (k_2-1-n)!\ l!} \\ & \times \frac{1}{2^{\mathrm{d}(n+l+m-1)/2}\ (2+n+l+m)^{\mathrm{d}/2}}\ , \end{aligned} \tag{15}$$

where $c = \rho_0 W_-$ denotes again the average connectivity.

The above expression has been evaluated numerically and is represented in Figure 1 for $d = 3$ and $c = 6$. There exist obviously connectivity correlations in the sense that particles of low coordination are surrounded more likely by other low-connected particles. Similarly, particles of high coordination are likely to be surrounded by other high-coordinated particles. This effect can be understood intuitively: Low coordination of a particle i corresponds to a small number of other particles inside the effective crosslinking volume W_- centered in $\mathbf{R}_i^0$. Due to the overlap of this volume with the crosslinking volume of the neighboring particles, these will typically have a small number of potential crosslinking partners, too. The curves in Figure 1 cross 1 in the vicinity of $k_2 \simeq c+1$, which is the average connectivity of particles found by considering endpoints of randomly chosen crosslinks.

Connectivity correlations decrease exponentially with spatial dimension d and vanish in the limit $d \to \infty$. In this limit, the crosslink network becomes a random graph in the sense of [18].

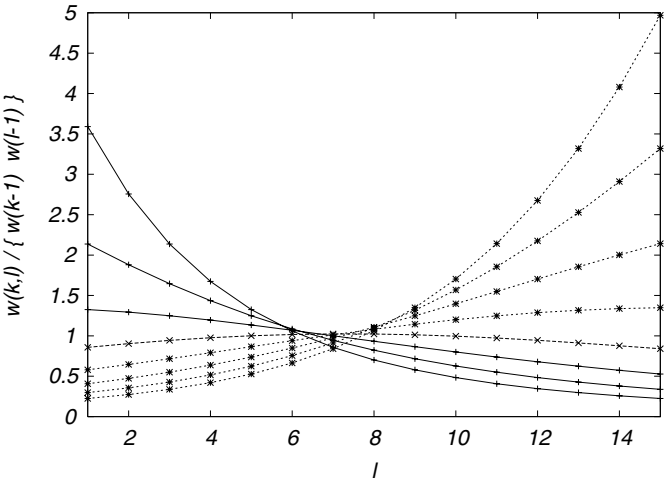

Fig. 1. Connectivity correlations for $d = 3$ and average connectivity $c = \rho_0 W_- = 6$. The figure shows the probability that a randomly selected crosslink has endpoints of connectivities k resp. l, as a function of l for various values of $k = 1, 3, 5, 7, 9, 11, 13, 15$ (from top to bottom on left axis, lines are guides to the eyes), and normalized by the uncorrelated probability $w(k-1)w(l-1)$. Values larger than one correspond to positive correlations, values smaller than one to anti-correlations.

3.4 Small loops

Another signature of the finite-dimensional structure of the crosslink network is the existence of an extensive number of short loops and other local, non-treelike sub-graphs. For example, the mean number of triangles is easily computed,

$$\begin{aligned} \mathcal{N}_\Delta &= \sum_{i<j<k} \overline{J_{ij}J_{jk}J_{ki}} \\ &= \binom{N}{3} \overline{J_{12}J_{23}J_{13}} \\ &= \binom{N}{3} \int \frac{\mathrm{d}^d R_1^0\ \mathrm{d}^d R_2^0\ \mathrm{d}^d R_3^0}{V^3}\ p(\mathbf{R}_1^0 - \mathbf{R}_2^0) \\ &\quad \times p(\mathbf{R}_2^0 - \mathbf{R}_3^0)\ p(\mathbf{R}_1^0 - \mathbf{R}_3^0) \\ &= \frac{N}{6}\rho_0^2 \int \mathrm{d}^d R_1^0\ \mathrm{d}^d R_2^0\ p(\mathbf{R}_1^0)\ p(\mathbf{R}_2^0)\ p(\mathbf{R}_1^0 - \mathbf{R}_2^0) \\ &= \frac{N}{6}\rho_0^2 W_\Delta\ . \end{aligned} \tag{16}$$

and seen to be *extensive* for generic short ranged distributions $p(\mathbf{R})$. For the particular choice of equation (9) we find $\rho_0^2 W_\Delta = \rho_0^2 (2\pi/\sqrt{3}a)^d = c^2 3^{-d/2}$. For constant average connectivity, the number of triangles tends to zero as $d \to \infty$. In this limit we recover the properties of random graphs, which are known to be locally tree-like.

The presented derivation can be easily generalized to more complicated local structures, always giving rise to extensive numbers decreasing exponentially with growing spatial dimension.

4 Mayer-cluster expansion of the replicated local density function

After having discussed some geometrical properties of the random networks generated according to finite-dimensional percolation, we go back to the original physical model of a crosslinked fluid, as given by equation (1). We discuss the order parameter of the gel phase and show how to compute local static density fluctuations within a Mayer-cluster expansion.

4.1 Localization of particles and the physical order parameter

As discussed previously [8,11,13], the sol-gel transition is an equilibrium phase transition from a liquid state (sol) to an amorphous solid state (gel). In the gel a finite fraction of particles is localized in the vicinity of fixed equilibrium positions. Increasing the number of crosslinks, localization first occurs, when a macroscopic cluster of crosslinked molecules appears, *i.e.* at the percolation threshold. Hence the fraction of localized particles is determined by the mass of the macroscopic cluster.

Due to the random crosslinks, the equilibrium positions of the localized particles do not exhibit any periodic structure, but are random. The gel is an amorphous solid, but still all macroscopic properties have to be translationally invariant. In particular, the single-particle density

$$\rho^{(1)}(\mathbf{r}) = \sum_{i=1}^{N} \overline{\langle \delta(\mathbf{r} - \mathbf{R}_i)\rangle} = \rho_0 \tag{17}$$

is homogeneous in both phases. Here and in the following, the thermal average with respect to the equilibrium state of the crosslinked system, (equation (4)), is denoted by $\langle\cdot\rangle$.

To detect localization, one has to consider higher moments of the local density. The simplest one is

$$\rho^{(2)}(\mathbf{r}^1, \mathbf{r}^2) = \sum_{i=1}^{N} \overline{\langle \delta(\mathbf{r}^1 - \mathbf{R}_i)\rangle \langle \delta(\mathbf{r}^2 - \mathbf{R}_i)\rangle} \,. \tag{18}$$

Macroscopic homogeneity implies that $\rho^{(2)} = \rho^{(2)}(\mathbf{r}^1 - \mathbf{r}^2)$. In the sol phase, all particles are free to explore the whole container and hence any particular one is equally likely to be in any sub-volume. This implies $\langle \delta(\mathbf{r}^1 - \mathbf{R}_i)\rangle = 1/V$ and hence $\rho^{(2)} = \rho^{(2)}(\mathbf{r}^1 - \mathbf{r}^2) = \rho_0/V$. In the gel phase, however, a finite fraction of all particles is part of the macroscopic cluster and thus localized. In the simplest model [12], one assumes Gaussian localization $\langle \delta(\mathbf{r}^1 - \mathbf{R}_i)\rangle \propto \exp\{-(\mathbf{r}^1 - \mathbf{a}_i)^2/(2\xi_i^2)\}$ around homogeneously distributed random localization centers $\mathbf{a}_i$. Here ξ_i is the localization length, characterizing the extent of thermal fluctuations around the preferred position $\mathbf{a}_i$. The second moment is then given by

$$\rho^{(2)}(\mathbf{r}^1 - \mathbf{r}^2) = \frac{}{\displaystyle\sum_{i=1}^{N} \int \frac{\mathrm{d}^d a_i}{(2\pi\xi_i^2)^d V} \exp\left\{-\frac{(\mathbf{r}^1 - \mathbf{a}_i)^2}{2\xi_i^2} - \frac{(\mathbf{r}^2 - \mathbf{a}_i)^2}{2\xi_i^2}\right\}}$$
$$= \rho_0 \int_0^\infty \mathrm{d}\xi^2 \tilde{P}(\xi^2) \left(\frac{1}{4\pi\xi^2}\right)^{\frac{d}{2}} \exp\left\{-\frac{(\mathbf{r}^1 - \mathbf{r}^2)^2}{4\xi^2}\right\}. \tag{19}$$

The second moment is thus expressed in terms of the distribution of localization lengths

$$\tilde{P}(\xi^2) := \frac{1}{N} \sum_{i=1}^{N} \overline{\delta(\xi^2 - \xi_i^2)} \tag{20}$$

which is expected to be rather broad due to the inhomogeneous environment of different particles: Some particles are expected to be strongly localized due to high local connectivity (steep local potentials), whereas particles *e.g.* on dangling bonds are expected to exhibit larger spatial fluctuations, corresponding to larger localization lengths.

The gelation transition occurs, when the connectivity per particle is $\mathcal{O}(1)$. Hence, there is no reason to assume Gaussian static density fluctuations, and the second moment (18) is not sufficient to completely characterize the structure of the gel phase. Instead, the full distribution of local static density fluctuations is required, or, equivalently, all moments

$$\rho^{(l)}(\mathbf{r}^1, \ldots \mathbf{r}^l) = \sum_{i=1}^{N} \overline{\prod_{j=1}^{l} \langle \delta(\mathbf{r}^j - \mathbf{R}_i)\rangle} \,. \tag{21}$$

Within mean-field theory, it has been shown that all higher moments can be expressed in terms of $P(\xi^2)$, according to

$$\rho^{(l)}(\mathbf{r}^1, \ldots \mathbf{r}^l) = \rho_0 \int \mathrm{d}^d a \int_0^\infty \mathrm{d}\xi^2 \tilde{P}(\xi^2) \times \left(\frac{1}{2\pi\xi^2}\right)^{\frac{dl}{2}} \exp\left\{-\frac{1}{2\xi^2} \sum_{j=1}^{l} (\mathbf{r}^j - \mathbf{a})^2\right\} \tag{22}$$

so that the structure is characterized by a single function, the distribution of localization lengths. Whether or not this result holds beyond mean-field theory is an open question.

4.2 From the replicated partition function to an effective molecular fluid

Our aim is the computation of the partition function of equation (4). The most important pair potential U is the excluded volume interaction. It is known that the crosslinked melt without excluded volume will collapse. Hence we cannot simply set $U(R) = 0$. Here we introduce

instead a Lagrange parameter to ensure the constraint of homogeneous density. To this end we choose

$$-\beta U(R) = \int_{V^N} \mathrm{d}^{dN}x \ \mu(\mathbf{x}) \sum_i \delta(\mathbf{x} - \mathbf{R}_i) = \sum_i \mu(\mathbf{R}_i) \tag{23}$$

and consider $\mu(\mathbf{R})$ as a Lagrangian multiplier coupled to the single-particle density. It will be determined such that the single particle density remains homogeneous. Technically it is much simpler to work with single-particle potentials instead of the excluded volume interaction.

We expect the model to be self-averaging in the macroscopic limit, *i.e.* intensive observables should not depend on the particular disorder realization, but only on the statistical ensemble of crosslinks. Hence we set out to compute the disorder averaged free energy $F := -\overline{\ln Z(\mathcal{C})}$ with

$$Z(\mathcal{C}) = \int_{V^N} \mathrm{d}^{dN}R \ \exp\left\{ \sum_i \mu(\mathbf{R}_i) - \sum_{i<j} J_{ij} V(\mathbf{R}_i - \mathbf{R}_j) \right\} . \tag{24}$$

We use units of energy such that $\beta = 1$.

To perform the average over the crosslink distribution we use the replica trick [19]

$$\overline{\ln Z(\mathcal{C})} = \lim_{n\to 0} \frac{\overline{Z(\mathcal{C})^n} - 1}{n} , \tag{25}$$

first assuming positive integer n, and using a replica-symmetric ansatz to analytically continue the results to $n \to 0$ at the end. For integer n, the model is replaced by n copies $R^a, a = 1, ..., n$, with independent coordinates but identical disorder. We can explicitly calculate the average over the J_{ij}, for given R^0, and find

$$\begin{aligned}\overline{Z(\mathcal{C})^n} &= \int_{V^{nN}} \prod_{a=1}^{n} \mathrm{d}^{dN}R^a \\ &\quad \times \overline{\exp\left\{ \sum_i \sum_{a=1}^{n} \mu(\mathbf{R}_i^a) - \sum_{i<j} J_{ij} \sum_{a=1}^{n} V(\mathbf{R}_i^a - \mathbf{R}_j^a) \right\}} \\ &= \frac{1}{V^N} \int_{V^{(n+1)N}} \prod_{a=0}^{n} \mathrm{d}^{dN}R^a \exp\left\{ \sum_i \sum_{a=1}^{n} \mu(\mathbf{R}_i^a) \right. \\ &\quad \left. + \sum_{i<j} \ln\left[1 + p(\mathbf{R}_i^0 - \mathbf{R}_j^0) \left(\mathrm{e}^{-\sum_{a=1}^{n} V(\mathbf{R}_i^a - \mathbf{R}_j^a)} - 1 \right) \right] \right\} .\end{aligned} \tag{26}$$

Note that the integration in the last line runs also over all disorder configurations $\mathbf{R}_i^0$. It thus resembles an $(n+1)$-times replicated system, where the replica of index 0 corresponds to the liquid configuration being part of the quenched disorder, and the replicas $a = 1, ..., n$ are the thermal degrees of freedom of the crosslinked model.

The main idea is now to interpret this expression as the partition function of a fluid of N "effective molecules", each consisting of $n+1$ particles [20]. We simplify the notation by introducing a $d(n+1)$-dimensional vector $\hat{R}_i = (\mathbf{R}_i^0, ..., \mathbf{R}_i^n)$ for the position vectors of the "constituents" of molecule i. The molecules interact pairwise *via* the potential

$$V_n(\hat{R}_i - \hat{R}_j) = - \ln\left[1 + p(\mathbf{R}_i^0 - \mathbf{R}_j^0) \left(\mathrm{e}^{-\sum_{a=1}^{n} V(\mathbf{R}_i^a - \mathbf{R}_j^a)} - 1 \right) \right] , \tag{27}$$

which is symmetric with respect to permutations of the last n particles, thus reflecting the replica symmetry of the replicated partition function. Note that there are no explicit *intra*-molecular interactions. However, the *inter*-molecular interactions are many-particle interactions, thus leading to an effective coupling of different particles within one molecule. In the context of gelation, the central question is whether or not molecules are bound in the sense, that $|\mathbf{R}_i^a - \mathbf{R}_i^b|$, $a \neq b$, stays finite for a finite fraction of all molecules i in the thermodynamic limit. As we will see in the following, unbound molecules may be identified with the sol fraction, bound molecules with the gel fraction which appears only at or above the gelation transition.

4.3 Mayer-cluster expansion for the effective molecular fluid

Having in mind the interpretation of the replicated and (partially) disorder-averaged system as an effective fluid, we can use the classical concepts of equilibrium statistical mechanics of fluids [21], in particular the Mayer-cluster expansion in the diagrammatic formulation of [22]. We thus introduce the Mayer-bond

$$\begin{aligned} b(\hat{R}_i, \hat{R}_j) &= \mathrm{e}^{-V_n(\hat{R}_i - \hat{R}_j)} - 1 \\ &= p(\mathbf{R}_i^0 - \mathbf{R}_j^0) \left[\mathrm{e}^{-\sum_{a=1}^{n} V(\mathbf{R}_i^a - \mathbf{R}_j^a)} - 1 \right] , \end{aligned} \tag{28}$$

which factorizes into a n-fold replicated Mayer-bond of a fully connected system times the probability of existence of the crosslink $J_{ij} = 1$.

The quantity of central interest for gelation are the moments of the local density (21), all of which can be related to the single-*molecule* density

$$\rho(\hat{r}) = \sum_{i=1}^{N} \left\langle \delta(\hat{r} - \hat{R}_i) \right\rangle_n . \tag{29}$$

The brackets $\langle \cdot \rangle_n$ denote the thermodynamic average of the effective molecular fluid, (Eq. (26)). The moments of the local density $\rho^{(l)}(\mathbf{r}^1, ... \mathbf{r}^l)$ are obtained from the molecule density according to

$$\rho^{(l)}(\mathbf{r}^1, ..., \mathbf{r}^l) = \lim_{n\to 0} \int_V \mathrm{d}^d r^0 \prod_{a=l+1}^{n} \int_V \mathrm{d}^d r^a \ \rho(\hat{r}) . \tag{30}$$

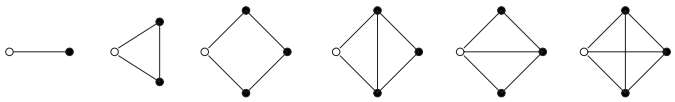

Fig. 2. Simplest diagrams in the Mayer-cluster expansion of the local replicated density. These diagrams are not reducible to two disconnected components by deleting a single vertex.

For a macroscopically translationally invariant system, as the gel, all single-*particle* densities have to be homogeneous, implying for the molecule density

$$\lim_{n\to 0}\int_{V^n} \mathrm{d}^d r^0 \cdots \mathrm{d}^d r^{a-1}\ \mathrm{d}^d r^{a+1}\cdots \mathrm{d}^d r^n\ \rho(\hat{r}) = \rho_0 \quad (31)$$

for all $a = 0, ..., n$, (Eq. (17)).

The following can be understood best by using a graphical representation. We consider diagrams whose vertices are either white circles, representing a molecule at position $\hat{r}$, or black circles, representing an integration over the single-molecule density. The lines connecting two circles denote a Mayer-bond $b(\hat{r}_1, \hat{r}_2)$. Each diagram has to be divided by its symmetry number which counts the number of possible permutations of vertices which do not alter the diagram. Simple examples are given in Figure 2, *e.g.* the first diagram reads $\int \mathrm{d}^{d(n+1)}\hat{r}_1 b(\hat{r}, \hat{r}_1)\rho(\hat{r}_1)$. The symmetry number equals 1 as black and white circles are distinguishable. Two circles are never connected by more than one Mayer-bond. A diagram will be called *one-vertex irreducible*, if it does not reduce to two disconnected diagrams by deleting any single vertex and its adjacent Mayer-bonds. All diagrams in Figure 2 are one-vertex irreducible.

Using the results of [22], $\rho(\hat{r})$ has to fulfill the nonlinear integral equation

$$\ln\rho(\hat{r}) = \mu(\hat{r}) + \sum \text{one-vertex irreducible diagrams with one white circle of coordinate } \hat{r}, \text{ and an arbitrary number of black circles.} \quad (32)$$

As already mentioned above, the single-particle potentials $\mu(\hat{r}) = \sum_a \mu(\mathbf{r}^a)$ act as Lagrangian multipliers guaranteeing the homogeneity condition (31). The first diagrams with up to four vertices are shown in Figure 2.

4.4 Structure of the density: Distribution of localization lengths

In order to extract the moments of the local density according to equation (30), we have to perform the replica limit $n \to 0$. We therefore introduce some ansatz on the analytical structure of $\rho(\hat{r})$. The first assumption concerns the validity of replica symmetry at the order-parameter level: We assume that $\rho(\hat{r})$ is invariant under any permutation of the n replicas $a = 1, ..., n$ of the crosslinked system. Only the disorder system $a = 0$ is distinct. The second assumption is inspired by the simple model of Gaussian localization of particles belonging to the gel. Following equation (22) we represent $\rho(\hat{r})$ by

$$\rho(\hat{r}) = (1-q)\frac{\rho_0}{V^n} + q\rho_0 \int \mathrm{d}^d R \int_0^\infty \mathrm{d}\tau_0\ d\tau\ P(\tau_0,\tau) \times \left(\frac{\tau_0}{2\pi}\right)^{\frac{d}{2}} \left(\frac{\tau}{2\pi}\right)^{\frac{dn}{2}} \exp\left\{-\frac{\tau_0}{2}(\mathbf{r}^0-\mathbf{R})^2 - \frac{\tau}{2}\sum_{a=1}^{n}(\mathbf{r}^a-\mathbf{R})^2\right\}. \quad (33)$$

The interpretation of this ansatz is quite simple: A fraction $1-q$ of effective molecules, with $0 \le q \le 1$, is not bound, the $n+1$ particles of each molecule are homogeneously distributed in V. The remaining qN molecules are restricted by the distribution of inverse squared localization lengths $P(\tau_0, \tau)$. Given a particular $\mathbf{r}^0$ from the disorder distribution, we find a randomly drawn $\mathbf{R}$ at an average squared distance $1/\tau_0$, which itself is the localization center of the other n particles. Non-zero τ and τ_0 thus correspond to bound molecules, or, more physically, to a situation where the particles are localized close to the original disorder configuration which was drawn before crosslinking. Thus, q denotes the gel fraction of the crosslinked material, *i.e.* the fraction of particles which are part of its solid component. The localization length ξ^2 of the phenomenological model (Sect. 4.1) is simply related to $\tau = 1/\xi^2$. Our ansatz generalizes the ansatz introduced in [12] for the Deam-Edwards distribution, with reduced permutation symmetry. Please note that it already implies a homogeneous single-particle density. Only the global normalization has to be enforced, thus we can fix $\mu(\hat{r}) = \mu$ to be a constant chemical potential.

Ansatz (33) in fact solves the Mayer-cluster expansion (32) for an appropriate choice of $P(\tau_0, \tau)$. This can be seen best by investigating the structure of the diagrams on the left-hand side of equation (32). Due to the Gaussian shape of the Mayer bonds (28) all integrations corresponding to black circles can be carried out, see Section 5 for specific examples. The resulting expression is again a (continuous) sum over Gaussian terms in the distances $(\mathbf{r}^a - \mathbf{R})$. Also the symmetry of ansatz (33) is preserved, because the Mayer-bonds are symmetric with respect to permutations of the thermal replicas $a = 1, ..., n$, too. The Mayer-cluster expansion thus leads, *via* comparing the coefficients of the Gaussian contributions of identical variance on both sides of equation (32), to a non-linear integral equation for $P(\tau_0, \tau)$.

To calculate the physical order parameter, we have to plug the replica-symmetric ansatz (33) into equation (30). This can be done for arbitrary moments of the local density. For the sake of clarity, we restrict the presentation to the second moment ($l = 2$), and find by direct integration over $\mathbf{r}^0, \mathbf{r}^3, ..., \mathbf{r}^n$ and $\mathbf{R}$

$$\rho^{(2)}(\mathbf{r}^1, \mathbf{r}^2) = (1-q)\frac{\rho_0}{V} + q\rho_0 \int_0^\infty \mathrm{d}\tau\ P(\tau)\left(\frac{\tau}{4\pi}\right)^{\frac{d}{2}} \exp\left\{-\frac{\tau}{4}(\mathbf{r}^1 - \mathbf{r}^2)^2\right\}. \quad (34)$$

The second moment depends on $P(\tau_0, \tau)$ only through the reduced distribution

$$P(\tau) := \int_0^\infty \mathrm{d}\tau_0 \; P(\tau_0, \tau) \tag{35}$$

of localization lengths of the thermal system. The same is true for all higher moments, implying that the information on τ_0 is not needed in the description of a gel. We therefore concentrate our attention on the properties of the reduced distribution $P(\tau)$ alone.

5 Truncations of the Mayer-cluster expansion

Based on the Mayer-cluster expansion, one could try to partially resum the series, developing *e.g.* a hypernetted-chain or Percus-Yevick approximation [21]. Due to unsolved problems in calculating the replica limit of general diagrams, this seems, however, not to be tractable. Furthermore the above summations are notoriously bad, as far as critical exponents are concerned. We therefore restrict our investigations to the simplest truncations of the series. As we will see in the following section, already the first diagram, consisting of one white, one black vertex and a single Mayer-bond, reproduces the results of mean-field theory.

In Section 5.2 we include the first correction: a triangular diagram with one white and two black circles, being completely connected by three Mayer-bonds. This diagram is shown as the second one in Figure 2. We will show, that the inclusion shifts the sol-gel transition to higher connectivities. The critical properties remain unchanged; we find the same critical exponents for the growth of the gel fraction and for the scaling function of the inverse squared localization lengths.

All diagrams containing more than one Mayer-bond decrease exponentially with the space-dimension d, making truncations more reliable in high dimensions. However, the Mayer-cluster expansion cannot be considered as a systematic expansion around the infinite-dimensional mean-field.

5.1 Back to mean-field theory

We start with the simplest non-trivial truncation of the Mayer-cluster expansion: only the leftmost diagram of Figure 2 will be included. Its contribution is denoted by Γ_- and is explicitly given by

$$\Gamma_- = \int_{V^{n+1}} \mathrm{d}^{d(n+1)}\hat{r}_1 \rho(\hat{r}_1) p(\mathbf{r}_1{}^0 - \mathbf{r}^0) \times \left[\mathrm{e}^{-\sum_{a=1}^n V(\mathbf{r}_1{}^a - \mathbf{r}^a)} - 1 \right] . \tag{36}$$

If the above expression is plugged into the truncated Mayer-cluster expansion, one obtains a non-linear integral equation for $P(\tau)$ (details are given in Appendix A)

$$1 - q + q \int_0^\infty \mathrm{d}\tau \; P(\tau) \mathrm{e}^{-\mathrm{i}\tau x} = \exp\left\{ -cq + cq \int_0^\infty \mathrm{d}\tau \; P(\tau) \exp\left(-\mathrm{i} \frac{\kappa\tau}{2(\kappa+\tau)} x \right) \right\}. \tag{37}$$

The above equation becomes exact, if we choose $p(\mathbf{R}_i^0 - \mathbf{R}_j^0) = c/N$ to be distance-independent, instead of connecting only particles, which are close in d-dimensional space. In fact, one can easily see that in the long-ranged case all higher diagrams in the Mayer-cluster expansion tend to zero in the thermodynamic limit, leaving only the first diagram.

By sending $x \to -\mathrm{i}\infty$, we find a simple relation for the gel fraction,

$$1 - q = \exp\{-cq\} \tag{38}$$

first derived in the context of gelation in [23]. It coincides with the size of the giant component in random graph percolation [18]. Equation (38) always has the solution $q = 0$, corresponding to the fluid state with a vanishing fraction of localized particles. At the critical value of the average connectivity, $c_{crit} = 1$, a second solution appears continuously, accounting for the finite fraction of particles in the macroscopic cluster. If we slightly increase the number of crosslinks beyond the percolation threshold, $c = 1 + \varepsilon$ ($0 < \varepsilon \ll 1$), we find $q = 2\varepsilon + O(\varepsilon^2)$, *i.e.* the gel fraction grows linearly with the distance from the transition.

The equation for $P(\tau)$ can be simplified if we substitute equation (38) into equation (37), expand the right-hand side, and invert the Fourier transform:

$$P(\tau) = \mathrm{e}^{-cq} \sum_{l=1}^\infty \frac{c^l q^{l-1}}{l!} \int_0^\infty \mathrm{d}\tau_1 \cdots \mathrm{d}\tau_l \; P(\tau_1) \cdots P(\tau_l) \times \delta\left(\tau - \sum_{i=1}^l \frac{\kappa\tau_i}{\kappa + \tau_i} \right). \tag{39}$$

In the critical region q is small so that the expansion on the right hand side can be truncated. The typical inverse squared localization length grows linearly with ε. This can be seen by rescaling it as $\tau = \varepsilon\kappa\theta$. We introduce the scaling function $\pi(\theta) = \varepsilon\kappa P(\varepsilon\kappa\theta)$ and expand (39) to second order in ε (see Appendix B)

$$(1 - 2\theta)\pi(\theta) = \theta^2 \pi(\theta) + \int_0^\theta \mathrm{d}\theta_1 \; \pi(\theta_1)\pi(\theta - \theta_1) \; . \tag{40}$$

The above equations (38) and (40) were derived previously as the saddle-point approximation for polymers crosslinked according to the Deam-Edwards distribution [12]. In that work, a melt of linear macromolecules was studied in contrast to the present work, which starts from a fluid of point particles. Since the gelation transition is a continuous phase transition with a diverging correlation length, the critical behavior of the two systems is the

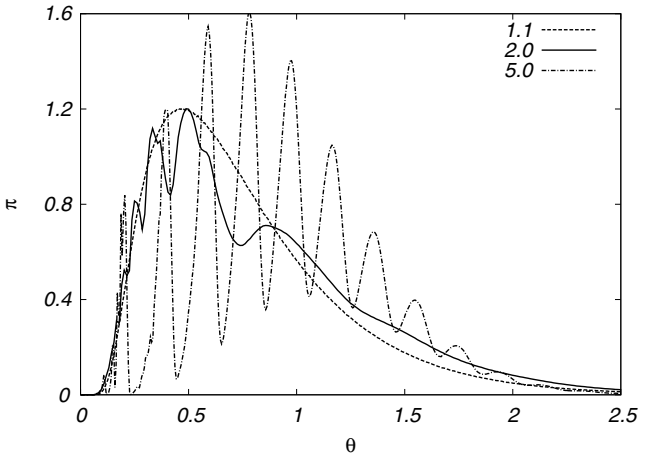

Fig. 3. Rescaled distribution $\pi(\theta) = (c-1)\kappa\, P((c-1)\kappa\theta)$ of inverse squared localization lengths, for average connectivities $c = 1.1,\ 2.0,\ 5.0$, and the simplest truncation of the Mayer-cluster expansion. The results are obtained numerically by the population dynamics for $\mathcal{M} = 10^6$ and $10^4\mathcal{M}$ iteration steps. We have tested that the iteration has reached a stationary point. The curves show the crossover from the smooth scaling function for small connectivities to the peaked structure for large connectivities.

same. This kind of universality with respect to the building blocks has been noticed previously [24] and in fact also holds for different crosslinking procedures.

The numerical solution of equation (40) in the critical region was given in reference [12], here we go on to a numerical solution of the full equation (39) for arbitrary connectivities. This numerical solution is based on a replica-symmetric variant of the population dynamics introduced in [25]. It starts with a large initial population $\mathcal{T} = \{\tau_1, ..., \tau_{\mathcal{M}}\}$ drawn randomly from some initial distribution $P_0(\tau)$, and the gel fraction q is determined from equation (38). The population is iterated in the following way:
(i) Draw a random positive integer l with probability $\mathrm{e}^{-cq}c^l q^{l-1}/l!$
(ii) Choose $l+1$ random integers $i_0, i_1, ..., i_l$ uniformly from $\{1, ..., \mathcal{M}\}$.
(iii) Replace τ_{i_0} by $\sum_{k=1}^{l} \kappa\tau_{i_k}/(\kappa + \tau_{i_k})$.
(iv) Go back to (i) with the updated population.
After a sufficiently large number of iterations, the histogram of $\mathcal{T}$ will be a good approximation of $P(\tau)$. For getting a better statistics, a time average over many iterations steps can be taken (starting after some waiting time needed for approaching a stable fix point).

We have implemented this algorithm, and calculated $P(\tau)$ for several values $c = \rho_0 W_-$ of the average connectivity. The results are shown in Figure 3. For connectivities close to the percolation threshold, $P(\tau)$ in fact follows the scaling function described by (40), and then starts to deviate and to develop a peak structure. Still, the typical values for the inverse squared localization lengths scale approximately like $c-1$. The peak structure observed for connectivities far beyond the gelation point becomes more and more pronounced, and allows for an analytical solution of the leading terms in $P(\tau)$ in the limit of high, but finite connectivity.

We realize that q approaches 1 exponentially for increasing c and the typical values of τ grow proportionally to c. Consequently we have

$$\sum_{i=1}^{l} \frac{\kappa\tau_i}{\kappa + \tau_i} = l\kappa + \mathcal{O}\left(\frac{l\kappa}{c}\right) \ . \tag{41}$$

Neglecting all subdominant terms, we find

$$P(\tau) \simeq \sum_{l=0}^{\infty} \mathrm{e}^{-c}\frac{c^l}{l!}\delta(\tau - l\kappa) \ . \tag{42}$$

Including also subdominant terms, the peaks are shifted by $\mathcal{O}(\kappa)$, whereas the width becomes $\mathcal{O}(c^{-1/2}\kappa)$, leading to the structure observed in the numerical solution for $P(\tau)$.

This leads to a very simple and attractive picture for strongly crosslinked systems: The localization length of a particle depends to leading order only on the number of crosslinks attached to the particle, or more precisely, its inverse square localization length equals the coordination times the crosslink strength. The distribution of localization lengths can then be written as a superposition of contributions of all coordinations l, each one occurring according to the Poisson distribution of equation (13), $w(l) = c^l\mathrm{e}^{-c}/l!$

An interesting consequence of the above interpretation arises in the context of the connectivity correlations discussed in Section 3.3: The same correlations transmit to the localization length. A weakly localized particle is, on average, surrounded by other weakly localized particles, a strongly localized one by other strongly localized particles. This kind of local inhomogeneities is also observed numerically for structural glasses, see [26]. Even though this picture is based on the simplest truncation of the Mayer-cluster expansion, we expect it to hold in the full theory (see the discussion in the next section).

5.2 First correction to mean-field

How does the inclusion of higher-order diagrams change the picture drawn above? We will give a partial answer by including also the triangular diagram Γ_Δ into the truncated Mayer series. The single-molecule density is then given by

$$\rho(\hat{r}) = \exp\{-\mu + \Gamma_- + \Gamma_\Delta\} \ . \tag{43}$$

The exponent on the rhs of equation (37) has thus to be completed by the term

$$\begin{aligned}\Gamma_\Delta \mapsto \frac{\rho_0^2 W_\Delta}{2}\int_0^\infty \mathrm{d}\tau_1\ \mathrm{d}\tau_2 \tilde{P}(\tau_1)\ \tilde{P}(\tau_2) \\ \times \sum_{\alpha_{1,2,3}\in\{0,\kappa\}} (-1)^{1+\frac{\alpha_1}{\kappa}+\frac{\alpha_2}{\kappa}+\frac{\alpha_3}{\kappa}} \\ \times \exp\left\{ -\mathrm{i}x\ \frac{\tau_1\tau_2(\alpha_1+\alpha_2)}{(\tau_1+\alpha_1+\alpha_3)(\tau_2+\alpha_2+\alpha_3)-\alpha_3^2}\right. \\ \left. + \frac{(\tau_1+\tau_2)(\alpha_1\alpha_2+\alpha_1\alpha_3+\alpha_2\alpha_3)}{(\tau_1+\alpha_1+\alpha_3)(\tau_2+\alpha_2+\alpha_3)-\alpha_3^2}\right\} \end{aligned} \tag{44}$$

where we use the abbreviation $\tilde{P}(\tau) = (1-q)\delta(\tau) + qP(\tau)$ for the localization-length distribution of all N particles, including the delocalized ones with $\tau = 0$. The constant W_Δ is given in equation (16). Even if the derivation is slightly more involved, it follows the ideas presented in Appendix B for Γ_-.

In the limit $x \to -\mathrm{i}\infty$, we obtain a closed equation for the gel fraction q,

$$1 - q = \exp\{-cq + \rho_0^2 W_\Delta q(1-q)\}\ . \tag{45}$$

Specializing to the Gaussian shape of $p(\mathbf{r}^0)$ given in (9), we find $\rho_0^2 W_\Delta = 3^{-d/2}c^2$. A nonzero gel fraction appears continuously at the critical value c_{crit} of the average connectivity given by

$$\gamma := \frac{2}{3^{\frac{d}{2}}} c_{\mathrm{crit}} = 1 - \sqrt{1 - 4\cdot 3^{-\frac{d}{2}}}. \tag{46}$$

For $d = 3$ we find $c_{\mathrm{crit}} = 1.3515$, and for increasing spatial dimension the critical connectivity decreases exponentially to one. So, in contrast to the simplest truncation, we find a dimension-dependent gelation point. The increasing number of needed crosslinks is due to the fact that the finite-dimensional disorder produces more compact structures (triangles, tetrahedra, etc.), and more links are needed to build up a macroscopic cluster of connected particles, see also Figure 4.

Increasing the connectivity c by a small amount ε above the percolation threshold, $c = c_c + \varepsilon$, we can expand equation (45) in both ε and q. Neglecting contributions of $\mathcal{O}(\varepsilon^k q^l)$ with $k + l \geq 3$, we find

$$q = 2\frac{1-\gamma}{1-\gamma c_{\mathrm{crit}}}\varepsilon + \mathcal{O}(\varepsilon^2)\ . \tag{47}$$

The gel fraction q starts to grow linearly with the distance from the transition; the critical exponent for the gel fraction is thus given by its mean-field value. Only the prefactor is changed, in 3 dimensions it equals 3.231. The prefactor approaches its mean-field value exponentially, as the spatial dimension is increased.

We expect the same critical exponent to be valid for any finite truncation of the Mayer-cluster expansion,

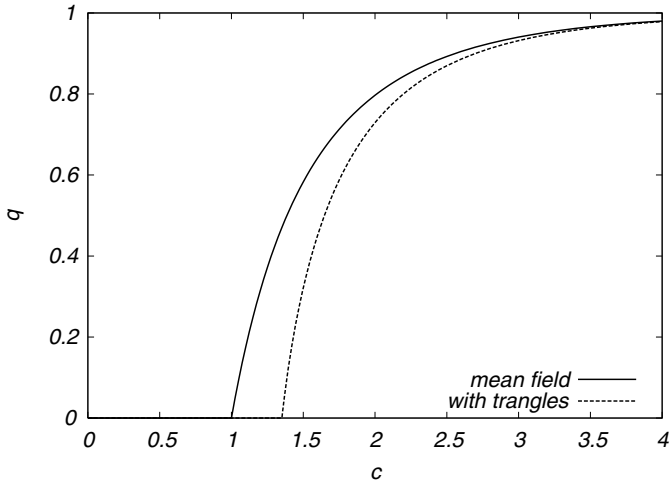

Fig. 4. Gel fraction as a function of the average connectivity $c = \rho_0 W_-$ for $d = 3$ and both truncations of the Mayer-cluster expansion. When the triangular diagram is included, the existence of a non-zero gel fraction sets in later.

because the equation determining the gel fraction has the form

$$1 - q = \exp\left\{\sum_{i=1}^{i_{\max}} a_i q^i\right\} \tag{48}$$

where $i_{\max}$ is the maximal number of black vertices in the considered diagrams. The gelation transition happens at $a_1 = 1$, implying a linear growth of the gel fraction. A different exponent can only result either from a resummation of an infinite series or if accidentally $a_2 = 1/2$ at the critical point, a situation which obviously would correspond to a very specific choice of the model parameters.

For general crosslink concentration c and the truncation including only the linear and triangular diagrams, the equation for the distribution of localization lengths follows from equations (43, 44). It can be written as a series expansion, similar to the mean-field result of equation (39). However, not all coefficients of the expansion are positive. Hence, these coefficients cannot be interpreted as probabilities any more, and the population dynamics cannot be applied.

We can still compute the distribution of localization lengths in the critical regime. The scaling function has to be modified according to

$$\pi(\theta) = \frac{1-\gamma}{1-\frac{2}{3}\gamma c_{\mathrm{crit}}}\varepsilon\kappa\ P\left(\frac{1-\gamma}{1-\frac{2}{3}\gamma c_{\mathrm{crit}}}\varepsilon\kappa\theta\right)\ . \tag{49}$$

Proceeding analogously to Appendix B, we reproduce equation (40) and hence find that the critical behavior of the distribution of inverse squared localization lengths remains unchanged by the triangular diagram.

Also the limiting case of high crosslink densities $c \gg 1$ is tractable. In particular, ansatz (42) still solves the integral equation up to corrections of $\mathcal{O}(c^0)$. To this end, we plug this ansatz into Γ_Δ as given in (44), and use that $\tau_{1,2} = \mathcal{O}(c)$ with a probability that approaches one for increasing c. Hence the argument of the exponential in (44)

is given by $-\mathrm{i}(\alpha_1+\alpha_2)x+\mathcal{O}(1/c)$ and does not depend on α_3 to leading order in $1/c$. The summation over α_3 thus leads to a cancellation of the leading order, such that $\Gamma_\Delta = \mathcal{O}(1/c)$, *i.e.* the triangular diagram does not contribute to the leading order in $1/c$ but only to the corrections of solution (42). We expect the same to hold also for higher-order diagrams.

More generally, we expect mean-field theory to give qualitatively correct results in the gel phase away from the critical point. The quantitative agreement becomes increasingly better for growing connectivity, as can be seen for the gel fraction (see Fig. 4) as well as for the distribution of localization length.

6 The Deam-Edwards distribution

Previous work on the statistical mechanics of gelation does not use the cluster statistics of percolation theory, but instead follows the elegant strategy of Deam and Edwards [6], who have given an implicit formula for the distribution of crosslinks, which is believed to be equivalent to finite dimensional percolation. It is the aim of this section to clarify the relation between the two approaches and put the Deam-Edwards distribution in a more general context.

We start from equation (5), but allow for fluctuations in the total number of crosslinks, assuming a Poisson distribution. A particular crosslink configuration is then constructed in three steps:

(1) Choose a configuration R^0 randomly, according to the distribution

$$\varphi(R^0) = \frac{\mathrm{e}^{-\psi(R^0)}}{\int \mathrm{d}^{dN}R\ \mathrm{e}^{-\psi(R)}}\ . \tag{50}$$

A natural choice would be $\psi(R^0)=U(R^0)$ in order to model instantaneous crosslinking of a fluid with correlations induced by the pair interactions $U(R^0)$. As we shall see, the Deam-Edwards distribution does not correspond to this choice.

(2) Given the configuration R^0, choose the total number of crosslinks M according to a Poisson distribution

$$W(M|R^0) = \frac{h(R^0)^M}{M!}\mathrm{e}^{-h(R^0)}\ , \tag{51}$$

where $h(R^0)$ is an arbitrary positive function.

(3) Given the configuration R^0 and the total number of crosslinks M, choose a crosslink configuration $\mathcal{C}=\{(i_e,j_e)\}_{e=1}^M$ with probability

$$P(\mathcal{C}|R^0,M) = \prod_{e=1}^{M} p(i_e,j_e|R^0,M)\ . \tag{52}$$

An observable $f(R^0,\mathcal{C})$, which depends not only on the crosslink configuration $\mathcal{C}$ but possibly also on R^0 is then averaged according to

$$\overline{f(R^0,\mathcal{C})} = \sum_{M=1}^{\infty}\prod_{e=1}^{M}\sum_{i_e,j_e=1}^{N}\int \mathrm{d}^{dN}R^0\varphi(R^0)\frac{(h(R^0))^M}{M!} \times \mathrm{e}^{-h(R^0)}P(\mathcal{C}|R^0,M)f(R^0,\mathcal{C})\ . \tag{53}$$

Modeling continuum percolation, we take $\varphi(R^0)=1/V$ and $h(R^0)=cN/2$ independent of R^0, so that the mean number of crosslinks $\overline{M}=cN/2$ is macroscopic and fluctuations around the average are small. The number of crosslinks per particle fluctuates around its finite mean c.

In the approach of Deam and Edwards, one argues that particles which have a high probability to be close in the fluid phase also have a high probability to be crosslinked. The corresponding distribution of crosslinks is defined implicitly through the average of an observable [6,7], according to

$$\overline{f(R^0,\mathcal{C})}^{DE} = \sum_{M=1}^{\infty}\frac{(\mu)^M}{M!} \times\prod_{e=1}^{M}\sum_{i_e,j_e=1}^{N}\frac{\int \mathrm{d}^{dN}R^0 e^{-U(R^0)}\prod_{e=1}^{M}\Delta(|\mathbf{R}^0_{i_e}-\mathbf{R}^0_{j_e}|)f(R^0,\mathcal{C})}{\int \mathrm{d}^{dN}R^0 e^{-U(R^0)+\mu\sum_{i,j=1}^{N}\Delta(|\mathbf{R}^0_i-\mathbf{R}^0_j|)}}. \tag{54}$$

Here $U(R^0)$ denotes the pair potential, acting among the particles of the fluid, and $\Delta(x)$ is a short-ranged, positive function. The Deam-Edwards distribution is a special case of the above more generally defined distribution of crosslinks (50–52), implying a special choice for $\varphi(R)$ and $h(R)$ denoted by $\varphi^{DE}(R)$ and $h^{DE}(R)$. To uniquely identify these functions we choose $f(R^0,\mathcal{C})=\delta(R^0-R)\delta(M-K)$ and compute its average according to equation (54)

$$\overline{\delta(R^0-R)\delta(M-K)}^{DE} = \frac{\left[\mu\sum_{i,j=1}^{N}\Delta(|\mathbf{R}_i-\mathbf{R}_j|)\right]^K}{K!} \times\frac{\mathrm{e}^{-U(R)}}{\int \mathrm{d}^{dN}R^0\quad \mathrm{e}^{-U(R^0)+\mu\sum_{i,j=1}^{N}\Delta(|\mathbf{R}^0_i-\mathbf{R}^0_j|)}}\ . \tag{55}$$

Computing the same average with the general class of distributions according to equation (53)

$$\overline{\delta(R^0-R)\delta(M-K)} = \frac{\mathrm{e}^{-\psi(R)}}{\int \mathrm{d}^{dN}R^0\quad \mathrm{e}^{-\psi(R^0)}}\frac{h(R)^K}{K!}\mathrm{e}^{-h(R)} \tag{56}$$

allows us to identify

$$\psi^{DE}(R) = U(R) - \mu\sum_{i,j=1}^{N}\Delta(|\mathbf{R}_i-\mathbf{R}_j|) \qquad \text{and}$$

$$h^{DE}(R) = \mu\sum_{i,j=1}^{N}\Delta(|\mathbf{R}_i-\mathbf{R}_j|). \tag{57}$$

We note that, first, the chemical potential of the crosslinks, which determines the total number of crosslinks, depends on the disorder configuration. A short ranged $\Delta(|\mathbf{R}|)$ will give rise to an intensive concentration, because $\sum_{i,j=1}^{N} \Delta(|\mathbf{R}_i - \mathbf{R}_j|)$ should be of order $\mathcal{O}(N)$. Fluctuations are expected to be of order $\mathcal{O}(\sqrt{N})$, so that one might hope that in the macroscopic limit it does not matter, whether $h(R)$ in the Poissonian distribution is taken to be constant or chosen to be R-dependent as by Deam and Edwards.

Second, the potential $\psi^{DE}(R)$, which determines the crosslink configuration, is *not* the potential of the underlying fluid as it should be for chemical gelation. In particular the correlations of the fluid should not depend on the function $\Delta(R)$ which determines the probability of a crosslink to be formed. The choice of Deam and Edwards has, however, technical advantages, because it simplifies replica calculations: The replica theory resulting from the above average (54) with $f(\mathcal{C}) = -\ln Z(\mathcal{C})$ is the only one which is symmetric with respect to permutations of all $n+1$ replicas. In view of the above identifications, this seems to be an artifact of the Deam-Edwards distribution and the generic theory of gelation will not have this additional symmetry, but will only be symmetric with respect to permutations of the n thermal replicas, as discussed in Section 4.4.

7 Conclusion

We have studied the gelation transition as well as the highly connected gel phase for crosslink distributions of d-dimensional percolation. The average over the random connectivity can be achieved with help of the replica trick. The resulting n-fold replicated, effectively uniform theory is interpreted as a molecular fluid, such that each particle of the unaveraged system corresponds to an effective molecule with $(n+1)$ constituents. The uniform theory is symmetric with respect to permutations of n replicas, which are introduced to represent $\ln Z$ and are called thermal replicas. One additional replica is used to generate short-range connectivity correlations and, in general, cannot be permuted with any of the thermal replicas.

The molecule density entails all information about the order parameter of the gel phase. "Bound" molecules indicate localization of the particles, in the sense that copies (or thermal replicas) of the original system are close to each other in real space. More precisely, the order parameter of the gel phase is the distribution of local static density fluctuations. This distribution is non-Gaussian due to the finite connectivity per particle. Hence moments of arbitrary order l are necessary to specify the state of the gel. Integrating the molecule density over all but l of the n thermal replicas, yields the lth moment of the local static density fluctuations.

The effective molecular fluid allows for an analysis in the framework of liquid-state theory. In particular a Mayer-cluster expansion can be set up for the local molecule density. The lowest-order term in the expansion yields back the results of mean-field theory. Assuming a replica-symmetric solution, we can compute corrections to mean-field theory. Here we do not concentrate on non-classical, critical behavior, which is difficult to obtain in such an expansion. Instead we focus on the properties of the gel phase away from the critical point. Within mean-field theory the structure of the gel is completely characterized by the distribution of localization lengths $P(\xi^2)$, which has been computed previously [12] in the critical region. Here we compute $P(\xi^2)$ for all connectivities and point out a one-to-one correspondence between the connectivity of a particle and its localization length. For high connectivities the distribution of localization lengths is shown to exhibit a multi-peak structure with the weight of each peak given by the Poisson statistics of connectivities.

Corrections to mean-field theory increase the percolation threshold, but do not change the qualitative picture of mean-field theory. In the limit of increasing connectivity the corrections to mean-field theory become less and less significant.

The analysis may possibly be extended to study two-point-correlation functions or even higher correlations. Given the connectivity correlations of neighboring sites, as discussed in Section 3.3, we expect to find similar correlations for strongly, respectively weakly localized particles. Another possible extension of our work concerns the elastic properties of the gel. It would certainly be interesting to compute the elastic constants within a Mayer-cluster expansion.

Besides the Mayer-cluster expansion, we have discussed a rather general class of crosslink distributions. This general framework helps to put the Deam-Edwards distribution in the context of percolation theory, and allows to study a variety of connectivity distributions. Whether or not the critical behavior is universal with respect to the distribution of the disorder is unknown and so far has hardly been addressed systematically in disordered systems.

Furthermore, the Deam-Edwards distribution was shown to be the only crosslink distribution giving rise to an average free energy which is symmetric with respect to permutations of $n+1$ replicas. The generic case – including percolation statistics as well as crosslinks with correlations of the melt – is symmetric with respect to permutations of the n thermal replicas only. In view of these results, it might be interesting to reconsider the issue of replica-symmetry breaking, which was shown to be absent in gels with the Deam-Edwards distribution [27].

We are grateful to Peter Müller for numerous comments on the manuscript. The work of AZ has been supported by the DFG through Grant No. Zi209/6-1 and SFB 1871.

Appendix A: Equation for $P(\tau)$ for the simplest truncated series

In this appendix, we derive the self-consistent equation for $P(\tau)$ from the simplest non-trivial truncation of the

$$\Gamma_- \to -cq + cq \int_0^\infty \mathrm{d}\tau_0 \; \mathrm{d}\tau \; P(\tau_0,\tau) \left(\frac{a\tau_0}{2\pi(a+\tau_0)}\right)^{\frac{d}{2}} \int_0^\infty \mathrm{d}\sigma_0 \; \delta\left(\sigma_0 - \frac{a\tau_0}{a+\tau_0}\right) \int_0^\infty \mathrm{d}\sigma \; \delta\left(\sigma - \frac{\kappa\tau_0}{\kappa+\tau}\right)$$
$$\times \left(\frac{2\pi}{\sigma_0 + n\sigma}\right)^{\frac{d}{2}} \exp\left\{-\frac{1}{4(\sigma_0+n\sigma)} \sum_{a,b=0}^{n} \sigma_a\sigma_b(\mathbf{r}^{\,a} - \mathbf{r}^{\,b})^2\right\}$$
$$\to -cq + cq \int_0^\infty \mathrm{d}\tau_0 \mathrm{d}\tau \; P(\tau_0,\tau) \int \mathrm{d}\sigma_0 \; \delta\left(\sigma_0 - \frac{a\tau_0}{a+\tau_0}\right) \int d\sigma \; \delta\left(\sigma - \frac{\kappa\tau}{\kappa+\tau}\right) \exp\left\{-\frac{1}{4\sigma_0} \sum_{a,b=0}^{n} \sigma_a\sigma_b(\mathbf{r}^{\,a} - \mathbf{r}^{\,b})^2\right\} \; .$$

Mayer-cluster expansion for the lth moment

$$\rho^{(l)}(\mathbf{r}^{\,1},...,\mathbf{r}^{\,l}) = \lim_{n\to 0} \int_V \mathrm{d}^d r^0 \prod_{a=l+1}^{n} \int_V \mathrm{d}^d r^a \exp\{-\mu + \Gamma_-\} \; . \quad \text{(A.1)}$$

We compute Γ_- with the ansatz of equation (33)

$$\rho(\hat{r}) = (1-q)\frac{\rho_0}{V^n} + q\rho_0 \int \mathrm{d}^d R \int_0^\infty \mathrm{d}\tau_0 \; \mathrm{d}\tau \; P(\tau_0,\tau) \times \left(\frac{\tau_0}{2\pi}\right)^{\frac{d}{2}} \left(\frac{\tau}{2\pi}\right)^{\frac{dn}{2}} \exp\left\{-\sum_{a=0}^{n} \frac{\tau_a}{2}(\mathbf{r}^{\,a} - \mathbf{R})^2 \; , \right\} \quad \text{(A.2)}$$

where we have introduced $\tau_a := \tau$, for all $a = 1, ..., n$. The ansatz is first simplified by integrating over $\mathbf{R}$

$$\rho(\hat{r}) = (1-q)\frac{\rho_0}{V^n} + q\rho_0 \int_0^\infty \mathrm{d}\tau_0 \; \mathrm{d}\tau \; P(\tau_0,\tau) \times \left(\frac{\tau_0}{\tau_0+n\tau}\right)^{\frac{d}{2}} \left(\frac{\tau}{2\pi}\right)^{\frac{dn}{2}} \times \exp\left\{-\frac{1}{4(\tau_0+n\tau)} \sum_{a,b=0}^{n} \tau_a\tau_b(\mathbf{r}^{\,a} - \mathbf{r}^{\,b})^2\right\} \; , \quad \text{(A.3)}$$

and then it is plugged into the expression for Γ_-

$$\Gamma_- = \int \mathrm{d}^{d(n+1)}\hat{r}_1 \rho(\hat{r}_1) p(\mathbf{r}_1{}^0 - \mathbf{r}^{\,0}) \times \left[\mathrm{e}^{-\sum_{a=1}^{n} V(\mathbf{r}_1{}^a - \mathbf{r}^{\,a})} - 1\right] \; . \quad \text{(A.4)}$$

We use harmonic interactions $V(\mathbf{r})$ and a Gaussian-shaped $p(\mathbf{r})$ to find

$$\Gamma_- = -\rho_0 W_- + \rho_0(1-q) \int \frac{\mathrm{d}^{d(n+1)}\hat{r}_1}{V^n} \times p(\mathbf{r}_1{}^0 - \mathbf{r}^{\,0}) \exp\left\{-\frac{\kappa}{2}\sum_a (\mathbf{r}_1{}^a - \mathbf{r}^{\,a})\right\}$$
$$+ \rho_0 q \int \mathrm{d}^d R \int_0^\infty \mathrm{d}\tau_0 \; d\tau \; P(\tau_0,\tau) \left(\frac{\tau_0}{2\pi}\right)^{\frac{d}{2}} \left(\frac{\tau}{2\pi}\right)^{\frac{dn}{2}} \times \int \mathrm{d}^{d(n+1)}\hat{r}_1 \; \exp\left\{-\frac{\tau_0}{2}(\mathbf{r}_1{}^0 - \mathbf{R})^2 - \frac{\tau}{2}\sum_{a=1}^{n}(\mathbf{r}_1{}^a - \mathbf{R})^2 - \frac{a}{2}(\mathbf{r}_1{}^0 - \mathbf{r}^{\,0})^2 - \frac{\kappa}{2}\sum_{a=1}^{n}(\mathbf{r}_1{}^a - \mathbf{r}^{\,a})^2\right\} \; . \quad \text{(A.5)}$$

The integrals over $\hat{r}_1$ are Gaussian and hence can be performed. We are interested in the leading term in the limit $n \to 0$, and hence replace $C^n \to 1$ with C an arbitrary constant. In this way we obtain

$$\Gamma_- \to -\rho_0 W_- q + \rho_0 q \int \mathrm{d}^d\mathbf{R} \int_0^\infty \mathrm{d}\tau_0 \mathrm{d}\tau P(\tau_0,\tau) \left(\frac{\tau_0}{a+\tau_0}\right)^{\frac{d}{2}} \times \exp\left\{-\frac{a\tau_0}{2(a+\tau_0)}(\mathbf{r}^{\,0} - \mathbf{R})^2 - \frac{\kappa\tau}{2(\kappa+\tau)}\sum_{a=1}^{n}(\mathbf{r}^{\,a} - \mathbf{R})^2\right\}$$
$$\to -cq + cq \int_0^\infty \mathrm{d}\tau_0 \; \mathrm{d}\tau \; P(\tau_0,\tau) \left(\frac{a\tau_0}{2\pi(a+\tau_0)}\right)^{\frac{d}{2}} \times \int_0^\infty \mathrm{d}\sigma_0 \; \delta\left(\sigma_0 - \frac{a\tau_0}{a+\tau_0}\right) \int \mathrm{d}\sigma \; \delta\left(\sigma - \frac{\kappa\tau_0}{\kappa+\tau}\right) \times \int \mathrm{d}^d R \quad \exp\left\{-\frac{\sigma_0}{2}(\mathbf{r}^{\,0} - \mathbf{R})^2 - \frac{\sigma}{2}\sum_{a=1}^{n}(\mathbf{r}^{\,a} - \mathbf{R})^2\right\} \; .$$

The $\mathbf{R}$-integration can be carried out, yielding

See equation above.

We have introduced $\sigma_a = \sigma$ for $a = 1, ..., n$ and have removed trivial n-dependencies which are irrelevant in the replica limit $n \to 0$.

$$\pi(\theta) = \mathrm{e}^{-cq} \sum_{l=1}^{\infty} \frac{c^l q^{l-1}}{l!} \int \mathrm{d}\theta_1 \cdots \mathrm{d}\theta_l \; \pi(\theta_1) \cdots \pi(\theta_l) \; \delta\left(\theta - \sum_{i=1}^{l} \frac{\theta_i}{1+\varepsilon\theta_i}\right)$$
$$= (1-2\varepsilon)(1+\varepsilon) \int \mathrm{d}\theta_1 \; \pi(\theta_1) \; \delta\left(\theta - \theta_1(1-\varepsilon\theta_1) + O(\varepsilon^2)\right)$$
$$+(1-2\varepsilon)(1+\varepsilon)^2\varepsilon \int \mathrm{d}\theta_1 \mathrm{d}\theta_2 \; \pi(\theta_1) \; \pi(\theta_2) \; \delta\left(\theta - \theta_1(1-\varepsilon\theta_1) - \theta_2(1-\varepsilon\theta_2) + O(\varepsilon^2)\right) + O(\varepsilon^2)$$
$$= (1-\varepsilon) \int \mathrm{d}\theta_1 \; \pi(\theta_1) \; \delta\left(\theta - \theta_1(1-\varepsilon\theta_1)\right) + \varepsilon \int \mathrm{d}\theta_1 d\theta_2 \; \pi(\theta_1) \; \pi(\theta_2) \; \delta(\theta - \theta_1 - \theta_2) + O(\varepsilon^2)$$
$$= \pi(\theta) + \varepsilon \left\{ -\pi(\theta) + 2\theta\pi(\theta) + \theta^2\pi'(\theta) + \int \mathrm{d}\theta_1 \; \pi(\theta - \theta_1)\pi(\theta) \right\} + O(\varepsilon^2) \; .$$

In order to obtain an equation for $P(\tau)$, the above expression is plugged into equation (A.1). For the sake of clarity, we only consider $l = 2$

$$\rho^{(2)}(\mathbf{r}^1, \mathbf{r}^2) = \lim_{n\to 0} \int_V \mathrm{d}^d r^0 \prod_{a=3}^{n} \int_V \mathrm{d}^d r^a \exp\{-\mu + \Gamma_-\} \; . \tag{A.6}$$

and note that all higher moments lead to the same equation for $P(\tau)$. The integrations over $\mathbf{r}^0$ and $\mathbf{r}^a$, $a = 3, ..., n$, can be carried out by expanding the exponential on the rhs of equation (A.6). The result

$$\rho^{(2)}(\mathbf{r}^1, \mathbf{r}^2) = \mathrm{e}^{-\mu - cq} \sum_{l=0}^{\infty} \frac{(cq)^l}{l!} \int_0^{\infty} \mathrm{d}\tau_1 \cdots \mathrm{d}\tau_l P(\tau_1) \cdots P(\tau_l)$$
$$\times \int_0^{\infty} \mathrm{d}\sigma \delta\left(\sigma - \sum_{i=1}^{l} \frac{\kappa\tau_i}{\kappa + \tau_i}\right)$$
$$\times \left(\frac{\sigma}{4\pi}\right)^{\frac{d}{2}} \exp\left\{-\frac{\sigma}{4}(\mathbf{r}^1 - \mathbf{r}^2)^2\right\}$$

depends only on the reduced distribution $P(\tau) = \int \mathrm{d}\tau_0 \; P(\tau_0, \tau)$ of inverse squared localization lengths of the crosslinked system. For the left hand side of the last equation we use expression (34) and compare coefficients of Gaussians of the same variance. In the last step, we adjust μ to fix the normalization and find

$$(1-q)\delta(\tau) + qP(\tau) =$$
$$\mathrm{e}^{-cq} \sum_{l=0}^{\infty} \frac{(cq)^l}{l!} \int_0^{\infty} \mathrm{d}\tau_1 \cdots \mathrm{d}\tau_l P(\tau_1) \cdots P(\tau_l) \delta$$
$$\times \left(\tau - \sum_{i=1}^{l} \frac{\kappa\tau_i}{\kappa + \tau_i}\right) \cdot \tag{A.7}$$

Taking the Fourier transform with respect to τ, allows us to evaluate the sum on the rhs of equation (A.7) and leads to equation (37).

Appendix B: Scaling function for the truncated series

In order to derive the scaling function for the distribution of localization lengths in the critical region, we start from the full equation (39) for the simplest truncated Mayer expansion, or equivalently for the mean-field theory:

$$P(\tau) = \mathrm{e}^{-cq} \sum_{l=1}^{\infty} \frac{c^l q^{l-1}}{l!}$$
$$\times \int_0^{\infty} \mathrm{d}\tau_1 \cdots \mathrm{d}\tau_l \; P(\tau_1) \cdots P(\tau_l) \; \delta\left(\tau - \sum_{i=1}^{l} \frac{\kappa\tau_i}{\kappa + \tau_i}\right) . \tag{B.1}$$

The critical connectivity is given by $c = 1$. If we further increase the number of crosslinks, $c = 1 + \varepsilon$ ($0 < \varepsilon \ll 1$), a macroscopic gel component appears. Its fraction is given by

$$q = 2\varepsilon + O(\varepsilon^2) \; . \tag{B.2}$$

Moreover, the inverse squared localization lengths, *i.e.* the τ's, are expected to grow linearly with the distance from the critical point. We thus rescale $P(\tau)$ by setting $\tau = \varepsilon\kappa\theta$, and define the distribution

$$\pi(\theta) = \varepsilon\kappa P(\varepsilon\kappa\theta) \; . \tag{B.3}$$

Plugging this into equation (B.1), we find

See equation above.

The first non-trivial order thus gives the expected integro-differential equation (40) for the scaling function $\pi(\theta)$.

References

1. Classical contributions are described in P.J. Flory, *Principles of Polymer Chemistry* (Cornell University Press, Ithaca, 1953)
2. D. Stauffer, J. Chem. Soc., Faraday Trans. II **72**, 1354 (1976)
3. P.G. de Gennes, *Scaling Concepts in Polymer Physics* (Cornell University Press, Ithaka, 1979)
4. M. Adam, M. Delsanti, J.P. Munch, D. Durand, J. Phys. France **48**, 1809 (1987)

5. P.G. de Gennes, J. Phys. France **38**, L-355 (1977)
6. R.T. Deam, S.F. Edwards, Phil. Trans. R. Soc. A **280**, 317 (1976)
7. R.C. Ball, S.F. Edwards, Macromolecules **13**, 748 (1980)
8. P.M. Goldbart, N. Goldenfeld, Phys. Rev. Lett. **58**, 2676 (1987); Phys. Rev. A **39**, 1402 (1989); *ibid.* **39**, 1412 (1989)
9. S.V. Panyukov, JETP Lett. **55**, 608 (1992).
10. S.V. Panyukov, Y. Rabin, Phys. Rep. **269**, 1 (1996)
11. P.M. Goldbart, A. Zippelius, Phys. Rev. Lett. **71**, 2256 (1993)
12. H.E. Castillo, P.M. Goldbart, A. Zippelius, Europhys. Lett. **28**, 519 (1994)
13. P.M. Goldbart, H. Castillo, A. Zippelius, Adv. Phys. **45**, 393 (1996)
14. W. Peng, P.M. Goldbart, Phys. Rev. E **61**, 3339 (2000); W. Peng, P.M. Goldbart, A.J. McKane, Phys. Rev. E **64**, 031105 (2001)
15. H.K. Janssen, O. Stenull, Phys. Rev. E **64**, 026119 (2001)
16. M.P. Solf, T.A. Vilgis, J. Phys. A **28**, 6655 (1995)
17. B. Bollobas, *Random graphs* (Academic Press, London, 1985)
18. P. Erdős and A. Rényi, Magyar Tud. Akad. Mat. Kut. Int. Kőzl. **5**, 17 (1960); reprinted in: The Art of Counting edited by J. Spencer (MIT Press, Cambridge, MA, 1973)
19. S.F. Edwards, in *Polymer networks*, edited by A.J. Chrompff, S. Newman (Plenum, New York, 1971)
20. P.M. Goldbart, J. Phys. Cond. Matt. **12**, 6585 (2000)
21. C.A. Croxton, *Liquid state physics - A statistical mechanics introduction* (Cambridge University Press, 1974)
22. T. Morita, K. Hiroike, Prog. Theor. Phys. **25**, 537 (1961)
23. A. Zippelius, P.M. Goldbart, N. Goldenfeld, Europhys. Lett. **23**, 451 (1993)
24. M. Huthmann, M. Rehkopf, A. Zippelius, P. Goldbart, Phys. Rev. E **54**, 3943 (1996)
25. M. Mézard, G. Parisi, Eur. Phys. J. B **20**, 217 (2001)
26. K. Vollmayr-Lee, W. Kob, K. Binder, A. Zippelius, J. Chem. Phys. **116**, 5158 (2002)
27. P.M. Goldbart, A. Zippelius, J. Phys. A **27**, 6375 (1994)